Cell Surface Expansion in Polarly Growing Root Hairs of *Medicago truncatula*[1]

Sidney L. Shaw, Jacques Dumais, and Sharon R. Long*

Howard Hughes Medical Institute, Department of Biological Sciences, Stanford University, Stanford, California 94305–5020

Fluorescent microspheres were used as material markers to investigate the relative rates of cell surface expansion at the growing tips of *Medicago truncatula* root hairs. From the analysis of tip shape and microsphere movements, we propose three characteristic zones of expansion in growing root hairs. The center of the apical dome is an area of 1- to 2-μm diameter with relatively constant curvature and high growth rate. Distal to the apex is a more rapidly expanding region 1 to 2 μm in width exhibiting constant surges of off-axis growth. This middle region forms an annulus of maximum growth rate and is visible as an area of accentuated curvature in the tip profile. The remainder of the apical dome is characterized by strong radial expansion anisotropy where the meridional rate of expansion falls below the radial expansion rate. Data also suggest possible meridional contraction at the juncture between the apical dome and the cell body. The cell cylinder distal to the tip expands slightly over time, but only around the circumference. These data for surface expansion in the legume root hair provide new insight into the mechanism of tip growth and the morphogenesis of the root hair.

Cellular morphogenesis is the process by which a single cell obtains shape (Harold, 1990; Fowler and Quatrano, 1997). For walled cells growing under internal pressure, morphogenesis involves coupling the deposition of new wall materials with deformation of the existing cell wall. The balance between polymer incorporation, wall mechanical properties, and turgor pressure defines how a cell will expand and how, in multicellular organisms, individual cells contribute to tissue, organ, and organismal shape and form. The familiar box-shaped cells found in maturing plant tissues undergo diffuse expansion in local concert to produce tissue growth without unwanted mechanical stresses and buckling. Polarly growing root hairs, free of surrounding cells, extend into the local environment by highly focused tip growth. Both cell types must balance wall extension with wall tension to effect cellular expansion while avoiding catastrophic explosion. As a first step toward understanding how cellular shape generation is controlled in plant cells, we have measured the cell surface expansion of growing root hairs in the model legume *Medicago truncatula*.

Root hairs initiate as a small bulge from root epidermal trichoblast cells and elongate by the polarized addition of cell wall materials at the growing tip (Miller et al., 1997). Tip-growing cells concentrate secretory vesicles toward the apical end and create a tip-localized calcium gradient proposed to modulate vesicle fusion with the plasma membrane (Miller et al., 1992; Bibikova et al., 1997). Cytoskeletal elements running the length of the hair cell keep the nucleus and vesicle-rich cytoplasm near the growing apex (Lloyd et al., 1987). Mitochondria and Golgi elements are also localized toward the growing tip, providing energy and materials for growth (Miller et al., 1997). The consequence of continued polar growth is an elongated, cylindrical cell projecting outwardly from the root axis (Bibikova et al., 1997). The elongated hair-like morphology increases the exposed cell surface area important for water and nutrient uptake (Gilroy and Jones, 2000).

The expanding cell wall is composed of polysaccharide and a small percentage of protein (Carpita and Gibeaut, 1993; Cosgrove, 1997a). The wall matrix contains large cellulose microfibrils interlinked by smaller chains of xyloglucan containing polysaccharides termed hemicellulose (McCann et al., 1990). The cross-linked cellulose microfibril lattice is believed to provide the majority of tensile strength in mature walls (Cosgrove, 1997b; Arioli et al., 1998; Whitney et al., 1999) and, when aligned to one axis of the cell, might be responsible for restricting cellular expansion along that axis (Green, 1980). A variety of polygalacturonic acid-containing polysaccharides, collectively known as pectins, form a calcium cross-bridged gel that affects the wall porosity and cell rigidity. Pectins, hemicellulose, and glycoproteins are secreted into the wall via Golgi-derived vesicles, whereas cellulose is synthesized from cytoplasmic UDP-glucose and extruded into the wall (Kudlicka and Brown, 1997). Protein, mostly in the form of highly glycosylated proteoglycans, can affect the mechanical properties of the wall by acting as cross-linking agents between polymers (Brisson et al., 1994)

[1] S.R.L. is an investigator of the Howard Hughes Medical Institute. Additional support for this project was provided by the National Science Foundation/Faculty Award to Women (grant no. DCB–9024330 to S.R.L.).

* Corresponding author; e-mail Sharon.Long@stanford.edu; fax 650–725–8309.

or by increasing the amount of local wall expansion (Fry, 1995; McQueen-Mason and Cosgrove, 1995).

As pointed out by Green (1965), how a cell obtains shape cannot be inferred from the shape itself, but must be determined by measuring local rates of wall expansion during growth. If we consider the growing cell wall as a patchwork of squares, then the final shape of the cell is determined by both the rate at which each square expands and by the degree to which each square becomes more rectangular over time. The same final morphology can be obtained in different ways by varying local expansion rates and the degree of expansion anisotropy during growth.

The rate of wall expansion is measured as the fractional increase in area over time (i.e. the relative elemental rate [Erickson and Goddard, 1951; Castle, 1957; Green, 1973]) and is the sum of the linear relative expansion rates centered at one point on the cell, measured along perpendicular axes (Fig. 1c). The expansion anisotropy is expressed as the expansion rate along one axis divided by the expansion rate along the perpendicular axis. For an axisymmetric cell, such as the root hair, morphogenesis can be described using the rate of area expansion and the degree of expansion anisotropy along the growth axis.

We have measured the local cell wall expansion in root hair cells of the model legume, *M. truncatula* (Cook, 1999). Our choice of organism reflects an interest in the morphogenetic changes and eventual infection of legume root hairs by the nitrogen-fixing bacteria of the Rhizobiaceae family (Ridge, 1993). From measurements of material points on the expanding cell surface, we have calculated relative elemental rates of expansion as a function of position on the cell. We find that the local rates of expansion do not follow a simple model of decreasing isotropic expansion from apex to base (Green, 1973). What emerges is a more complex description of tip growth whereby the growing cell is slightly blunted at the very tip and the maximum growth rates are achieved in an annulus surrounding the cell apical pole where the curvature is highest. Furthermore, we demonstrate anisotropic wall expansion in the flank of the apical dome. From these observations, we propose several hypotheses for how the root hair cell is shaped during the process of growth.

RESULTS

Root Hair Growth

The general growth habit of *M. truncatula* root hairs in buffered nodulation medium (BNM) was documented using digital time lapse DIC microscopy (Figs. 2 and 3). Cells imaged at 10-min intervals for 15 h in liquid medium exhibited constant polar growth perpendicular to the root axis (Fig. 2). The

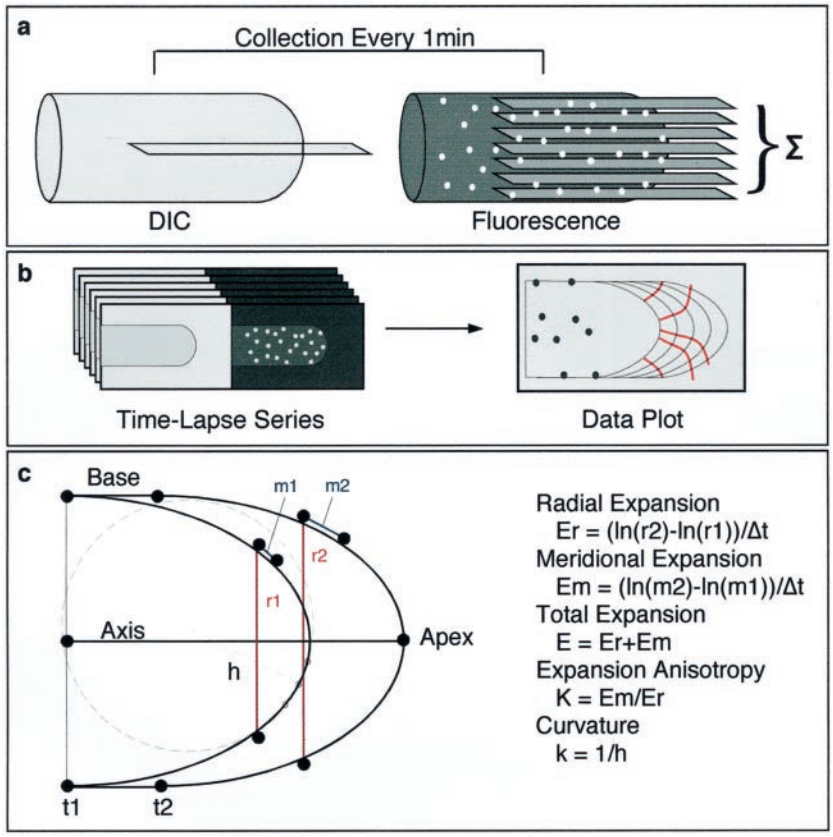

Figure 1. Imaging and data analysis. Time-lapse microscopy of growing root hairs was performed by taking a single differential interference contrast (DIC) image in the mid-plane of the cell and seven fluorescence images as an axial series at 1.5-μm intervals (a). Fluorescence series were projected to a single plane by summation and paired with the DIC image from the same time point (b). Microsphere and cell perimeter positions were extracted using semi-automated software (c). Distance measurements were taken from extracted data points and relative elemental rates were calculated as described. Curvature was determined by dividing cell perimeters into equally spaced divisions, and finding the radius of a circle (h) fit to three adjacent points on the perimeter.

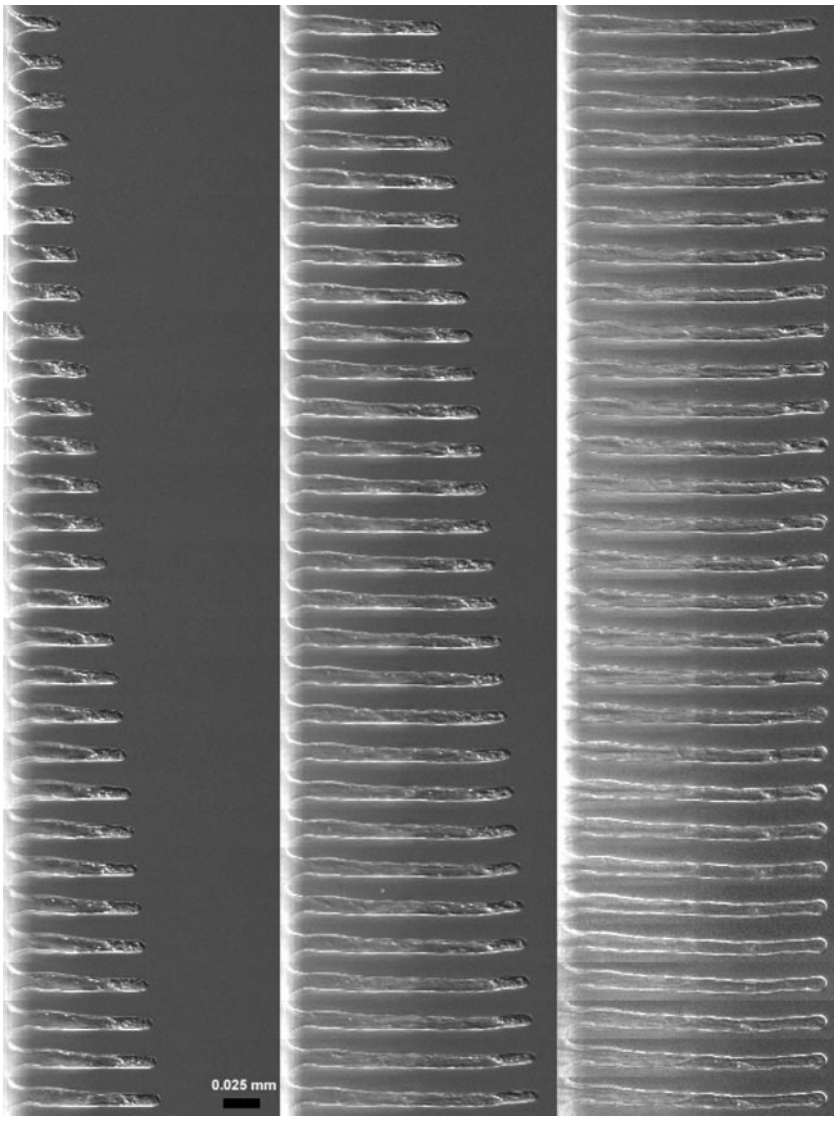

Figure 2. Time lapse of root hair growth. A single *M. truncatula* root hair from a 2-d-old seedling imaged at 10-min intervals for 15 h under constant perfusion. Extension is constant and nearly perpendicular to the root axis. Nutation, observed as small deviations from the principal growth axis, occurs throughout the image series. The cytosol is visible toward the tip of the cell during growth and redistributes after growth has ceased. Note the nuclear movement from the growing tip region to the center portion of the cell in the last panel. Bar = 25 μm.

nucleus and cytosol remained forward in the growing cell and redistributed when growth ceased as discussed by Miller et al. (1997). Root hair growth (extension) rates measured at 1-min intervals were approximately constant, averaging 0.35 $\pm$ 0.03 μm/min (n = 4 cells in Fig. 4). The mean SD for extension rate was 0.07 μm/min. Growth rates under these conditions did not show measurable oscillation or gradual increases and decreases when imaged at 1-min intervals for 30 to 60 min.

The net growth trajectory was perpendicular to the root axis yielding a nearly straight cell (Fig. 2). However, when observed in time lapse, nutation around the central axis of the cell was observed (Figs. 2 and 3). Nutation appeared as slight turns away from the central axis perpendicular to the focal plane lasting 5 to 20 min in duration. The mean diameter of a mature root hair $>$ 60 μm in length, under these growth conditions, is 12.2 $\pm$ 1.7 μm (n = 30 cells from five plants). The mean SD of the cell diameter along the length of any single root hair is $\pm$2.6 μm. Off-axis growth did not result in significant misshaping of the hair cell or persistent redirection of the cell axis under these growth conditions. Hence, root hair growth in medium permissive for symbiotic bacterial interactions had no dramatic effect on growth rate or cell shape.

Shape of the Cell Apex

To quantify changes in tip shape that occurred during the time course of an experiment, we measured the local curvature of the cell periphery traced from time-lapsed DIC images (Fig. 4, E–H). A color-coded representation of tip curvature over time is presented to illustrate tip shape over the course (1-min intervals) of an experiment (Fig. 4, I–L). This depiction of cell shape clearly shows a region of sustained higher curvature on both sides of the cell apex. The maximum curvature is observed 1 to 3 μm

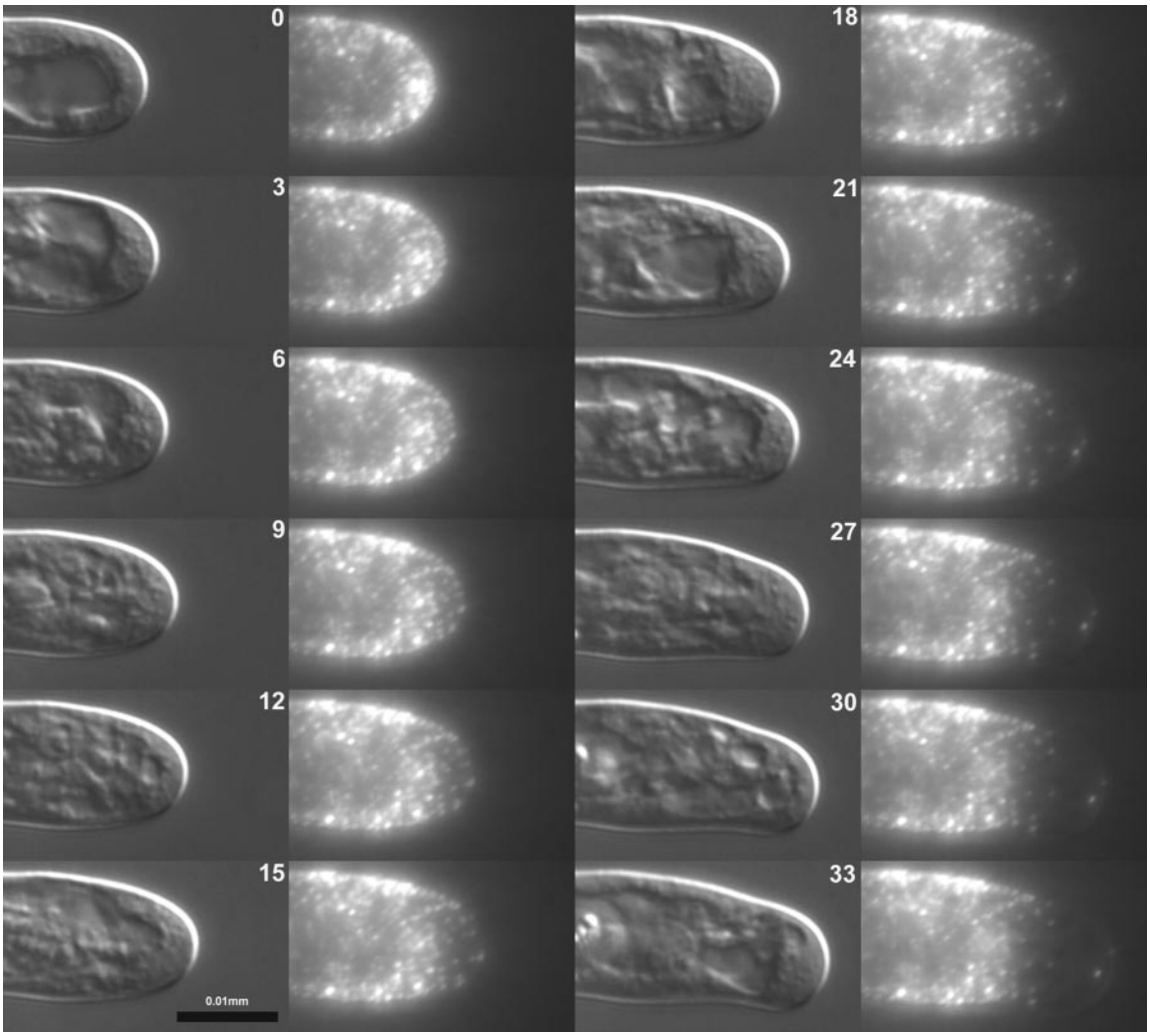

Figure 3. Time lapse of bead displacement on root hair surface. A single *M. truncatula* root hair was decorated with sub-resolution (0.1 μm) fluorescent microspheres and imaged using differential interference contrast and fluorescence microscopies. A time-lapsed series at 3-min intervals is shown representing 33 min of growth. The cell is beginning a small turn, characteristic of nutation, downward in the frame. Microspheres originating on the apical dome move relative to each other while microspheres adhering to the cell cylinder remain stationary. Time in minutes.

from the geometric tip of the cell (Fig. 5F). Hence, the general form of the cell apex is an elongated taper with a slightly blunted end.

Visible in this presentation of the data are several examples of reciprocal changes in curvature on opposite sides of the cell (e.g. Fig. 4K, 30–33 min) highlighting small-scale surges of off-axis growth. Cells undergoing a turn in the imaging plane due to nutation (Fig. 4, A and E) show a persistent increase in curvature on the side into which the cell is turning (Fig. 4I). It is interesting that the regions of high curvature become further separated in the nutating cell, creating a larger central region.

Root Hair Surface Expansion

To measure the local rates of cell surface expansion (relative elemental rates) that collectively describe cellular morphagenesis, we decorated individual root hair cells with 0.1-μm fluorescent microspheres and imaged the growing cells using digital time-lapse fluorescence microscopy (Figs. 3 and 4, A–D). The fluorescent microspheres serve as material markers on the cell surface from which measurements of expansion can be made by recording the changes in distance between microspheres. For this approach to be useful, we needed to assess whether the treatment intrinsically perturbs growth, and whether the microspheres remain fixed to the cell wall once applied. Microsphere application via a large bore micropipette had no measurable effect on cellular growth rate or morphogenesis (Fig. 3). Reversing the flow of the pipette used for microsphere application, revealed that the microspheres adhere to a matrix on the cell wall surface. Microspheres moved up to approximately 1.5 μm but returned to the original position

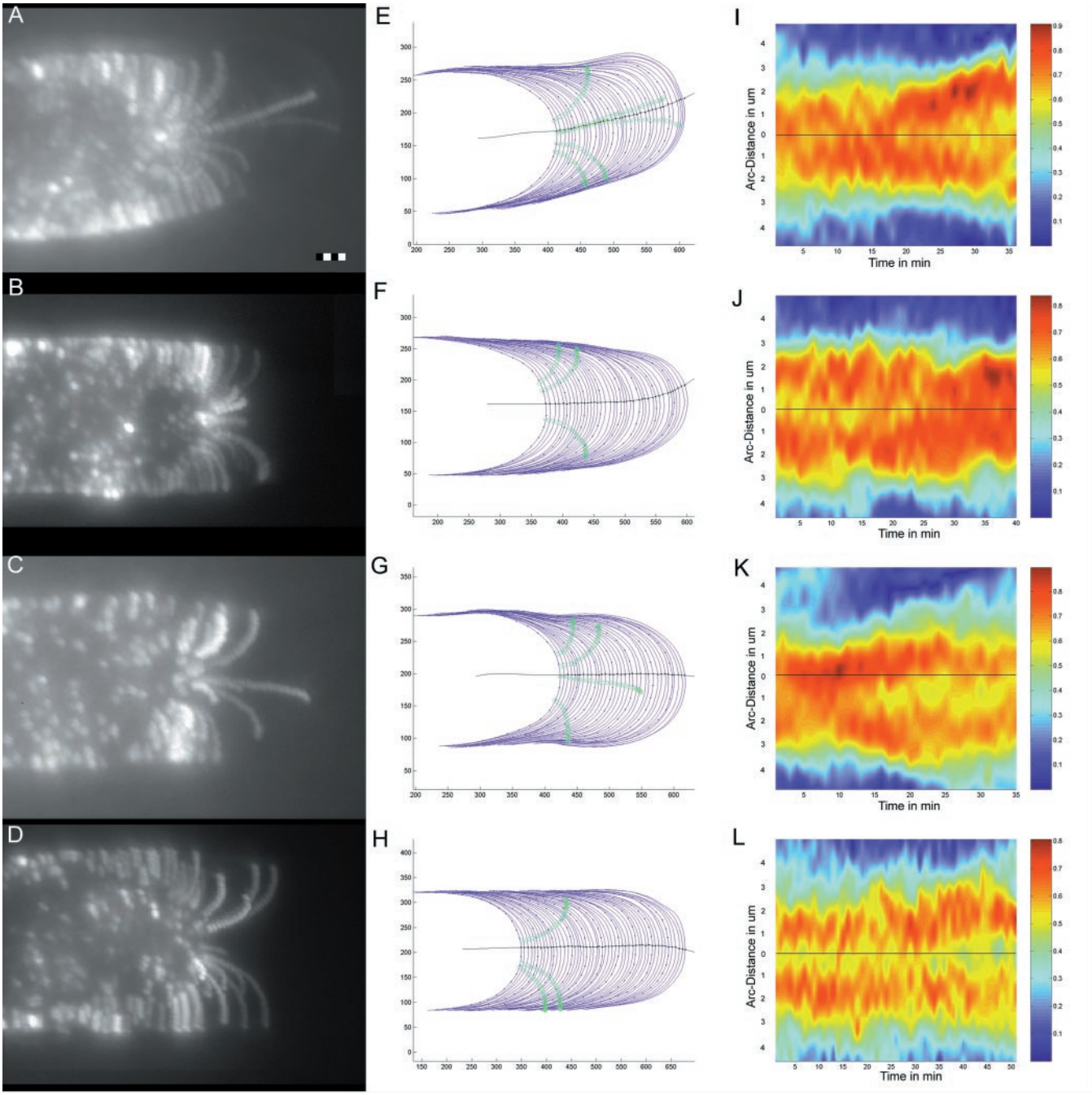

Figure 4. Data extraction and visualization. Time-lapsed image data (1-min interval) from four experiments. Summation images from time-lapsed fluorescence sequences (see "Materials and Methods") show the trajectories of all microspheres adhered to the surface of a growing root hair (A = 252 images summed [36 min × seven images], B = 280 images, C = 245 images, and D = 420 images). Bar = 2 μm. Cell perimeters from the associated DIC image series (blue lines) are plotted with the midline of the cell (black line) and the positions of microspheres from the fluorescence series (green circles) used for calculating relative rates of surface expansion. Scale represents pixel elements before conversion to micrometers (E–H). Dots have been placed at 1-μm intervals on every fifth cell perimeter in the outline for reference. Curvature of each cell perimeter at each time point is represented as a color-coded series (I–L). The center of the apex (black line in E–H) is drawn as a black line with the ordinate scale in micrometers. Curvature scales from low (blue) to high (red). Note the trough of lesser curvature at the cell center between two peaks of higher curvature distal to the cell apex.

on the hair after the pipette suction was stopped (data not shown). Attempts to move or dislodge microspheres permanently using either fluid streaming or fine-tipped micropipettes failed, indicating that the beads were fixed to the cell surface and reporting the underlying surface expansion.

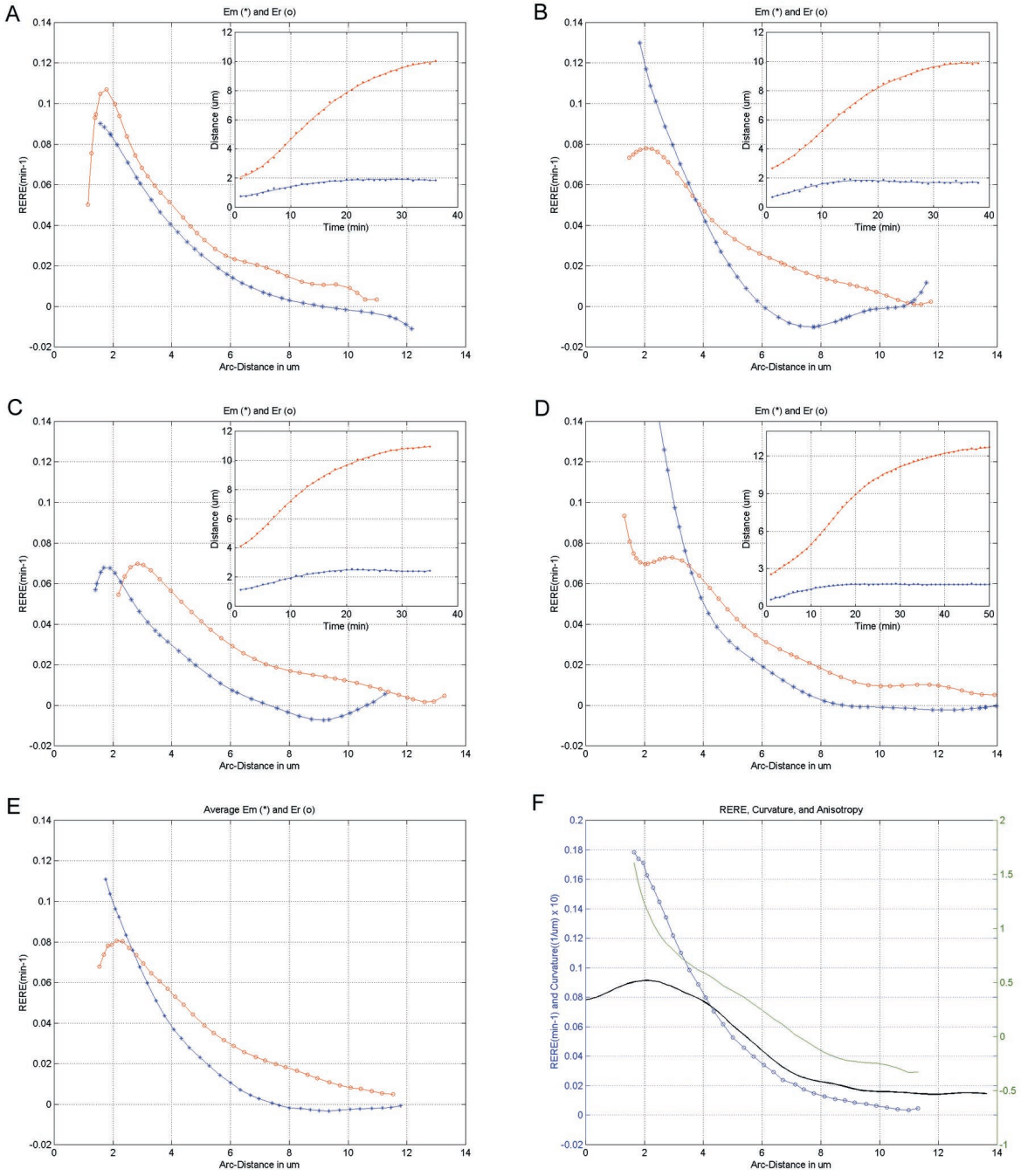

Figure 5. Relative elemental rates of expansion. The radial and meridional rates of surface expansion calculated from the distances between microspheres on a growing root hair tip (A–D). Rates (in min^{-1}) are plotted over the meridional distance in micrometers from the tip to the base of the apical dome. Red ○, Radial rates Er were calculated from a function fit to the distances between microspheres on the opposite sides of the apex (red line in inset). Blue *, Meridional rates (Em) were calculated using one of the same microspheres and an additional microsphere on the same side of the cell (blue line in inset). E, Mean Er and Em from A through D calculated by fitting all Em or Er data irrespective of tip size. Blue ○, Total expansion rate, obtained by adding the mean Em and Er, and growth anisotropy (green line), calculated by dividing Em/Er, are shown together with the mean curvature (black line) for A through D (F).

Relative elemental rates of expansion (RERE) (Fig. 5, A–D) were calculated using the change in distance between microspheres over time (Fig. 5, A–D, insets). RERE were calculated for cells that had, by chance, two microspheres traveling together on the same side of the cell and an additional microsphere traveling on

the opposite side so that both meridional (forward) and radial (width) expansion rates were obtained for the same cell (Fig. 1). Note that rates in Figure 5 (A–D) were obtained from plots depicted in Figure 4 (E–H). The position of microspheres on the cell surface was determined later by referencing the position of each microsphere with a cell perimeter traced from a DIC image acquired sequentially with each fluorescence series (Fig. 4, E–H).

Expansion rates within 1 to 1.5 μm of the apical pole likely increase slightly before decreasing toward the base of the apical dome (Fig. 5, A–D). Microspheres attaching within a 1-μm radius of the apical pole showed little movement away from the growth axis of the cell in the initial 10 to 15 min of the experiment ($n = 6$ cells in 23 experiments). Examples of a single microsphere (Fig. 4, C and G) and of two microspheres (Figs. 3 and 4, A and E) near the apical pole illustrate this phenomenon. Complete RERE were therefore not calculated because in no case were there paired microspheres for measuring radial expansion rates and the microsphere pairs for meridional rates moved too far (>4 μm) apart to assign rate accurately to a position on the cell surface. However, meridional RERE calculated within 2μm of the pole (first 15 min of experiment) using a microsphere at the pole and a microsphere elsewhere on the apical dome indicate that the RERE initially increases before decreasing toward the base of the cell (data not shown). This behavior can also be observed for the meridional rates of paired microspheres when very close to the pole (Figs. 4, C and G, and 5C). An additional estimate for expansion rate near the pole is given by the radial expansion rate very close to the apex. This assumption is made given that the two orthogonal rates (meridional and radial) must converge at the pole and that the radial expansion rate is the integral of all expansion between two particles when they are just flanking the pole. The radial rates actually decrease toward the cell apex (Fig. 5, A–D) providing further evidence that the maximum growth rates occur distal to the polar center of the cell.

Surface expansion 3 to 4 μm down the tip appears isotropic and approaches a maximum mean total value of 0.18 min^{-1} for the cells presented in this study (Fig. 5, E and F). This zone of high relative expansion rate coincides spatially with the region of highest mean curvature (Fig. 5F). Variation in RERE from cell to cell in this region of the tip is due primarily to small off-axis growth surges and to fluctuations in overall growth rate.

Growth in the remainder of the apical dome is characterized by dramatic expansion anisotropy (Fig. 5). Meridional and radial expansion rates begin to diverge at a point approximately 4 μm from the geometric tip (Fig. 5, A–D). This anisotropy arises when the meridional expansion rate falls to zero faster than the radial rate. Rates of meridional expansion falling below zero in the fitted data near the base of the apical dome indicate either no forward expansion or perhaps net contraction in this region. These rate data correspond to a slight movement of microspheres backward toward the root (Fig. 4, E–H). Radial expansion falls from a maximum 2 to 3 μm from the tip and exhibits a gradual decrease beginning halfway between the apex and the base.

Expansion of the Cell Body

Surface expansion beyond the apical dome (10–20 μm distal to the apical pole) was detectable when the average position of microspheres at the cell periphery was measured (see "Materials and Methods"). Microspheres near the cell periphery show a 50% to 200% higher SD of mean position perpendicular to the cell axis than parallel to the cell axis ($n = 4$ cells with four microspheres per cell for >20 images). This compares to a 15% difference in standard deviations of mean positions for microspheres resting near the cell midline. Hence, the microspheres are moving primarily outward, indicating that the cell is very gradually expanding circumferentially. This effect can be observed in the summation images as elongated microspheres at the cell periphery stretching perpendicularly to the cell axis (Fig. 4, A–D).

Visualization with Fluorescent Lectin

Microspheres remaining at the apical pole for extended time periods suggested that the central region of the apical dome might contain a rigid cap of nonexpanding material. To test this hypothesis, a fluorescently derivatized labeled lectin was applied to the cell wall in the same manner as the fluorescent microspheres. Root hair cells treated with the lectin fluoresced uniformly and grew with no obvious changes to growth rate or morphology (data not shown). Time-lapsed images of the lectin-coated cells during growth showed a gradual loss of fluorescence beginning at the tip of the cell. No significant residual staining was observed at the center of the apical dome during growth, suggesting that the central apical region is undergoing surface expansion. Images were of insufficient contrast to quantify fluorescence decay on the curved tip surface.

DISCUSSION

The root hair cell exhibits two dominant morphological characteristics. The hair projection is cylindrical, with a nearly constant diameter, and uniaxial, having little deviation from a straight line perpendicular to the root axis. How these simple elements of shape are created relies principally on growth at the cell apex. Therefore, to understand how the cell creates shape, we must determine the mechanisms by which growth is accomplished and, in this instance,

linked to cell polarity. With this first experimental study of cell surface expansion in the root hair, we have discovered zones of differing expansion rates and expansion anisotropy within the tip that suggest new hypotheses for the mechanism of root hair tip growth and creation of cell shape.

Surface Expansion at the Growing Tip

The most striking observation from this study of root hair tip growth is that the highest relative elemental rate of expansion is likely to be distal to the apical pole. This conclusion is drawn from two lines of evidence. First, microspheres landing close to the apical center show little initial movement perpendicular to the growth axis or with respect to each other. Estimates for expansion rates using these microspheres, and microspheres just flanking this region, suggest that the rates actually increase slightly before beginning to decrease 2 μm from the apical pole. No dramatic residual staining of the cell apex was observed using a fluorescently labeled lectin molecule, discounting the hypothesis that the apex is a rigid cap. In addition to the experiments using physical markers, measurements of tip curvature indicate a region of highest curvature distal to the apical center and corresponding to the areas where growth rates are estimated to be maximal. We believe that the regions of highest curvature flanking the pole respresent areas on the cell surface where the material is yielding more to internal pressure, i.e. where expansion rates are greater. From these observations, we propose that the apical 1 to 2 μm of the dome form a central zone that is expanding at a slower rate than the surrounding region. Hence, the highest expansion rates and greatest curvature occur in a region distal to the extreme apex, collectively forming an annular growth zone (Fig. 6).

The lower half of the apical dome is characterized by strong expansion anisotropy. The rate of radial expansion dominates the meridional rate beginning just distal to the zone of highest curvature and highest expansion rate. Surface expansion data from much larger algal rhizoid cells (Chen, 1973; Hejnowicz et al., 1977; Kataoka, 1982) show similar anisotropy in the tip flank. This tendency for material to expand more around the cell than forward could arise by different mechanisms. The amount of tension in the radial direction differs from the meridional direction due to the tendency for a cylindrical cell under pressure to expand against the smaller dimension. Thus the cell should require more reinforcement in the radial dimension, like hoops reinforcing a barrel, and could show growth anisotropy in response to increased stress in the radial direction. Therefore, the anisotropy could arise from a slowly cross-linking isotropic material caught in its own anisotropic stress gradient. Another explanation lies in the inherent nature of cellulose microfibrils to form an anisotropic material when co-aligned. If the cellulose were either laid down in ordered arrays or forced into a hoop-like alignment by the expanding surface (Green, 1973), the cell wall material itself would be expected to show anisotropic behavior regardless of strain anisotropy. Few data exist characterizing wall polymer supra-organization in the tips of legume root hairs (Newcomb and Bonnett, 1965; Emons and Wolters-Arts, 1983; Sherrier and VandenBosch, 1994; Miller et al., 1997), so it is not known to what degree cellulose is ordered or progressively cross-linked in these cells. To estimate the relative contributions of these mechanisms to the observed expansion anisotropy, we have undertaken a modeling study based on these data and the engineering theory of shells (J. Dumais, S.L. Shaw, C.R. Steele, and S.R. Long, unpublished data).

Expansion in the cell body distal to the apical dome is limited to small increases in the circumference. The growth rate in the barrel of the cell is small and might be more like growth in tissue-bound cells than a continuance of the polar growth process. Measurements of meridional expansion where the apical dome joins the barrel of the cell indicate that the material might be contracting slightly along the axis of the cell. The contraction is extremely small but could be indicative of a change in wall materials, such as crystallization of cellulose or the recycling of materials from the wall.

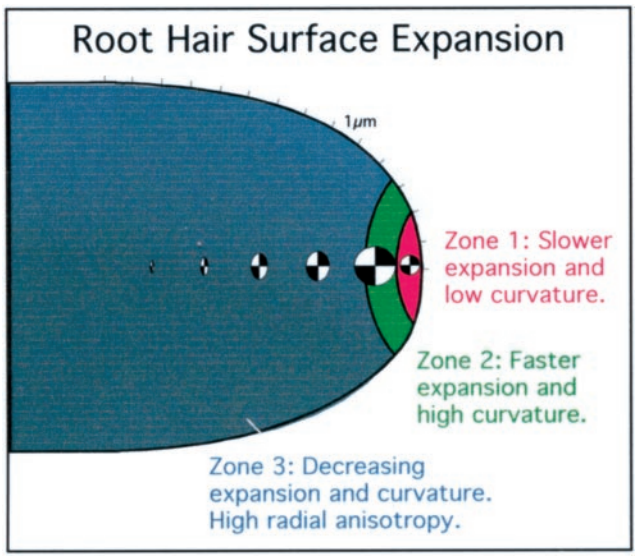

Figure 6. Proposed zones of surface expansion in the legume root hair. The root hair tip has been divided into three characteristic zones of surface expansion. The central zone (Zone 1) at the apex expands more slowly than the surrounding annular growth zone (Zone 2). Curvature reaches a global maximum at the annular growth zone (Zone 3), giving the appearance of slight shoulders to the outline of the cell. Growth in the flank of the expanding tip is anisotropic in nature, growing more in girth than in length. Circles indicate approximate relative elemental rates of surface expansion and expansion anisotropy.

Taken together, these observations provide a view of root hair tip growth substantively different from both previous descriptions (Green, 1973) and descriptions of tip growth in fungal hyphae (Bartnicki-Garcia et al., 1995). Tip growth in the legume root hair is not a simple system of isotropically expanding material deposited in a monotonic gradient (Green, 1973). The cell grows by small off-axis surges just distal to the apex that, in aggregate, form an annulus of forward-moving materials. Behind the annulus, expansion is nearly all for the purpose of increasing the diameter of the cell.

Cellular Morphogenesis

This description of the surface expansion associated with polar tip growth provides several clues to how the root hair achieves its final shape. The cell grows in a straight line when viewed over the course of several hours; however, when observed at shorter intervals, it continually lurches and turns from side to side. How the cell corrects small turns so that the net growth remains uniaxial likely relies on feedback within the apical growth annulus. We observed that when the cell does not correct the small, off-axis surge, a slight turn is initiated, resulting in nutation. Given that the area of highest curvature and maximum growth rate both fall within 2 to 3 microns of the tip apex, we envision this turn as being lead not by the apex apical pole per se, but rather by a local hot spot in the growth annulus. The cell bulges toward the direction it is turning but does not stop expanding on the opposite side of the apex. Hence, we propose that in order for the cell to remain on a given trajectory, there must be feedback control that keeps the expansion rate approximately equal around the annulus where growth is most prominent.

Cell expansion is axially symmetric, even when the cell is turning, suggesting that the signal for material deposition is a point source or symmetric around a pole. How the cell builds on that signal to create a cell of uniform diameter is partly explained by the highly anisotropic extension in the flank of the tip. The rate measurements indicate that the majority of forward (meridional) expansion occurs in the first third of the tip, generating cell extension. The remainder of the tip is expanding primarily in the radial direction. This expansion anisotropy must result from internal pressure working against the stiffness of the wall, and thus the cell is likely relying on turgor pressure and the material properties of the wall to create the mean diameter. How the cell more finely regulates the diameter is partly explained by the circumferential expansion discovered in the barrel of the cell. The various bends and indentations expected from nutation around the growth axis are effectively backfilled by the slight radial expansion.

MATERIALS AND METHODS

Plant Growth

Seeds from *Medicago truncatula* cv Jemalong were treated with 70% (v/v) ethanol for 40 min, rinsed twice in sterile water, and treated with full-strength commercial bleach for 40 min. After rinsing again in sterile water, seeds were imbibed for 4 h in water and germinated overnight in inverted, sealed Petri dishes. Seedlings were plated onto 1% (1 g per 100-mL volume; mass per volume) agarose containing no mass/volume BNM (Ehrhardt et al., 1992) and grown overnight at 24°C in the dark.

Microscopy

Seedlings 3 to 5 cm in length were mounted in custom perfusion chambers for imaging. The basal 1 cm of the plant root was perfused with BNM (5 mL/h) beginning >2 h prior to imaging. Fluorescent (red), sulfated polystyrene microspheres 0.1 μm in diameter (Sigma, St. Louis) were washed twice by centrifugation in distilled water, and suspended in BNM. Microspheres were applied via a large bore (20-μm i.d.) micropipette. Unattached microspheres were removed by reversing the pipette flow. Fluorescein-labeled *Ricinus communis* lectin (60-kD subunit, Sigma) was applied (1:100 dilution in BNM) in the same manner. Cells were imaged with a 60× 1.0 n.a. water immersion objective lens on an inverted microscope (TE200, Nikon, Melville, NY). A long working distance 0.85-n.a. condenser lens and high transmission polars (Nikon) were used for DIC microscopy. Fluorescence microscopy was performed with the DIC analyzer in place using a 100 W mercury arc light source and a Texas Red filter set (Chroma, Brattleboro, VT). Optical sectioning of the cell utilized a stepper motor controller and a z-axis focusing motor (LEP Ltd., Hawthorne, NY).

Cells were time-lapse imaged by autofocusing to the center plane of the cell in DIC mode, collecting a single DIC image, and collecting seven fluorescence images at 1.5-μm spacing from 4.5 μm above to 4.5 μm below the median cell plane (Fig. 1A). Images were collected with a cooled CCD camera (model 1300, Princeton Instruments, Trenton, NJ) at 12-bit precision through a 5× projection lens (Diagnostic Instruments, Sterling Heights, MI). Image acquisition, digital autofocus, and peripheral device control were automated using Metamorph imaging software (Universal Imaging Corporation, West Chester, PA).

Image Processing and Analysis

Processing and data extraction were performed using Metamorph and custom applications written in MATLAB v5.3 (Mathworks, Natick, MA) performed on an SGI-320 visual workstation (Silicon Graphics, Mountain View, CA). Stacks of seven fluorescence images, representing an axial series from a single time point, were projected into a single image by summation (Fig. 1A). The time-lapsed series was then aligned, to account for specimen drift, using three or more microspheres in the center of the cell >20 μm distal from the cell tip as fiducial points. Coordinates for align-

ment were used to align both the summation and DIC image series. For displaying all microsphere trajectories, a scaled, 8-bit representation of each summation image from the time-lapsed experiment was projected into a single 16-bit image by summation.

RERE were obtained by first plotting the positions of microspheres using the cell body as the frame of reference. Only microspheres in the central plane of the fluorescence series were used for analysis, limiting distance measurements to two dimensions. Microsphere position was recorded by selecting the microsphere center in the summation image at each time point. The distances between two microspheres moving on the same side of the cell, representing meridional distance, or on opposite sides of the cell, representing radial distance, were then measured (Fig. 1B). Error, arising predominantly from imprecision in determining the microsphere center and from slight microsphere "wobble" under perfusion, was estimated by measurements from a time-lapsed series of mature, nongrowing hairs ($\pm$1.1 pixels SD of the mean distance corresponding to $\pm$65 nm, $n = 25$ measurements on each of 12 sets of beads). To account for this error in the data collection, a line function was fit to the distance measurements using a seventh-degree polynomial. A stage micrometer was used for spatial calibration of the imaging system.

RERE were calculated by subtracting the natural logarithm of the distance at time point 1 from the natural logarithm of the distance at time point 2 and dividing by the time interval (Fig. 1B) as discussed by Peters and Bernstein (1997). This calculation is roughly equivalent to dividing the difference in distances between two microspheres at two time points by the mean of the distances for a given time interval. Total rates of expansion (E) were calculated by the addition of polynomial functions representing meridional expansion rates (Em) and radial expansion rates (Er) as a function of the distance from the center of the apex. Anisotropy (K) similarly was calculated by dividing Er by Em at each position. Rates were plotted with respect to cell surface position from apex to base, measured from the center of the apex (pole) to a position halfway between the two microspheres.

Perimeter outlines were generated by selecting points (30–50) on the cell outline from each DIC image in the time series, interpolating between the points, and window averaging through the entire outline. The center of the cell apex was determined from the extracted cell perimeters using the following algorithm. For each time point, the perimeter was divided into 23 equidistant points. Rays from each of the first 11 points were drawn to each of the last 11 points and the 121 midpoints from each time point were recorded. Fitting a line, using spline interpolation, for all midpoints from all time points creates a midline through the time-lapsed series that models the growth trajectory. Positions where the calculated midline intersects the cell perimeter correspond to the geometric center of the cell tip for the purposes of these analyses. Error in assignment of microspheres to perimeter position is estimated to be $\pm$0.20 μm. Curvature was determined by finding the radius of a circle circumscribing a triangle created using three equidistant points on the cell perimeter (Fig. 1B).

Expansion in the cell body was measured using microspheres at the periphery of the cell $>$20 μm from the apical center. Using the cell midline as the x axis of a Cartesian coordinate system, the standard deviations from the average positions of a particle in the X dimension and Y dimension were calculated. For comparison, measurements were made on microspheres resting near the middle of the cell rather than at the periphery.

ACKNOWLEDGMENTS

The authors wish to dedicate this work to the memory of Professor Paul Green. We thank Peter Ray for early suggestions and for comments on the manuscript.

Received May 25, 2000; accepted July 31, 2000.

LITERATURE CITED

Arioli T, Peng L, Betzner AS, Burn J, Wittke W, Herth W, Camilleri C, Hofte H, Plazanski J, Birch R, Cork A, Glover J, Redmond J, Williamson RE (1998) Molecular analysis of cellulose biosynthesis in Arabidopsis. Science **279:** 717–720

Bartnicki-Garcia S, Bartnicki DD, Gierz G (1995) Determinants of fungal cell wall morphology: the vesicle supply center. Can J Bot **73:** S372–S378

Bibikova T, Zhigilei A, Gilroy S (1997) Root hair growth in *Arabidopsis thaliana* is directed by calcium and an endogenous polarity. Planta **203:** 495–505

Brisson L, Tenhaken R, Lamb C (1994) Function of oxidative cross-linking of cell wall structural proteins in plant disease resistance. Plant Cell **6:** 1703–1712

Carpita NC, Gibeaut DM (1993) Structural models of primary cell walls in flowering plants: consistency of molecular structure with the physical properties of the cell during growth. Plant J **3:** 1–30

Castle E (1957) The topography of tip growth in a plant cell. J Gen Physiol **41:** 913–926

Chen JCW (1973) The kinetics of tip growth in the *Nitella rhizoid*. Plant Cell Physiol **14:** 631–640

Cook D (1999) *Medicago truncatula*: a model in the making! Curr Opin Plant Biol **2:** 301–304

Cosgrove D (1997a) Assembly and enlargement of the primary cell wall in plants. Annu Rev Cell Dev Biol **13:** 171–201

Cosgrove D (1997b) Relaxation in a high-stress environment: the molecular bases of extensible cell walls and cell enlargement. Plant Cell **9:** 1031–1041

Ehrhardt D, Atkinson EM, Long SR (1992) Depolarization of alfalfa root hair membrane potential by *Rhizobium meliloti* Nod factors. Science **256:** 998–1000

Emons A, Wolters-Arts AMC (1983) Cortical microtubules and microfibril deposition in the cell wall of root hairs of *Equisetum hyemale*. Protoplasma **117:** 68–81

Erickson R, Goddard DR (1951) An analysis of root growth in cellular and biochemical terms. Growth **10:** 89–116

Fowler J, Quatrano RS (1997) Plant cell morphogenesis: plasma membrane interactions with the cytoskeleton and cell wall. Annu Rev Cell Dev Biol **13:** 697–743

Fry S (1995) Polysaccharide-modifying enzymes in the plant cell wall. Annu Rev Plant Physiol Mol Biol **46:** 497–520

Gilroy S, Jones DL (2000) Through form to function: root hair development and nutrient uptake. Trends Plant Sci **5:** 56–60

Green PB (1965) Pathways of cellular morphogenesis, a diversity in *Nitella*. J Cell Biol **27:** 343–363

Green PB (1973) Morphogenesis of the cell and organ axis: biophysical models. Brookhaven Symp Biol **25:** 166–190

Green PB (1980) Organogenesis: a biophysical view. Annu Rev Plant Physiol Mol Biol **31:** 51–82

Harold F (1990) To shape a cell: an inquiry into the causes of morphogenesis of microorganisms. Microbiol Rev **54:** 381–431

Hejnowicz Z, Heinemann B, Sievers A (1977) Tip growth: patterns of growth rate and stress in the *Chara* rhizoid. Z Pflanzenphysiol Suppl **816:** 409–424

Kataoka H (1982) Colchicine-induced expansion of *Vaucheria* cell apex: alteration from isotropic to transversally anisotropic growth. Bot Mag Tokyo **95:** 317–330

Kudlicka K, Brown RM (1997) Cellulose and callose biosynthesis in higher plants. Plant Physiol **115:** 643–656

Lloyd C, Pearce KJ, Rawlins DJ, Ridge RW, Shaw PJ (1987) Endoplasmic microtubules connect the advancing nucleus to the tip of legume root hairs, but F-actin is involved in the basipetal migration. Cell Motil Cytoskelet **8:** 27–36

McCann MC, Wells B, Roberts K (1990) Direct visualization of cross-links in the primary plant cell wall. J Cell Sci **96:** 323–334

McQueen-Mason SJ, Cosgrove DJ (1995) Expanson mode of action on cell walls: analysis of wall hydrolysis, stress relaxation, and binding. Plant Physiol **107:** 87–100

Miller D, de Ruijter NCA, Emons AMC (1997) From signal to form: aspects of cytoskeleton-plasma membrane-cell wall continuum in root hair tips. J Exp Bot **48:** 1881–1896

Miller DD, Callaham DA, Gross DJ, Hepler PK (1992) Free Ca^{2+} gradient in growing pollen tubes of *Lilium*. J Cell Sci **101:** 7–12

Newcomb E, Bonnett HT (1965) Cytoplasmic microtubules and wall microfibril orientation in the root hairs of radish. J Cell Biol **27:** 575–589

Peters WS, Bernstein N (1997) The determination of relative elemental growth rate profiles from segmental growth rates. Plant Physiol **113:** 1395–1404

Ridge R (1993) A model of legume root hair growth and *Rhizobium* infection. Symbiosis **14:** 1–13

Sherrier DJ, VandenBosch K (1994) Secretion of cell wall polysaccharides in *Vicia* root hairs. Plant J **5:** 185–195

Whitney SEC, Gothard MGE, Mitchell JT, Gidley MJ (1999) Roles of cellulose and xyloglucan in determining mechanical properties of primary cell walls. Plant Physiol **121:** 657–663